Effect of Dynamic Stall, Finite Aspect Ratio and Streamtube Expansion on VAWT Performance Prediction using the BE-M Model

M. Raciti Castelli, A. Fedrigo and E. Benini

Abstract—A multiple-option analytical model for the evaluation of the energy performance and distribution of aerodynamic forces acting on a vertical-axis Darrieus wind turbine depending on both rotor architecture and operating conditions is presented. For this purpose, a numerical algorithm, capable of generating the desired rotor conformation depending on design geometric parameters, is coupled to a Single/Double-Disk Multiple-Streamtube Blade Element – Momentum code.

Both single and double-disk configurations are analyzed and model predictions are compared to literature experimental data in order to test the capability of the code for predicting rotor performance. Effective airfoil characteristics based on local blade Reynolds number are obtained through interpolation of literature low-Reynolds airfoil databases. Some corrections are introduced inside the original model with the aim of simulating also the effects of blade dynamic stall, rotor streamtube expansion and blade finite aspect ratio, for which a new empirical relationship to better fit the experimental data is proposed. In order to predict also open field rotor operation, a freestream wind shear profile is implemented, reproducing the effect of atmospheric boundary layer.

Keywords—Wind turbine, BE-M, dynamic stall, streamtube expansion, airfoil finite aspect ratio

I. INTRODUCTION AND BACKGROUND

THE use of Blade Element – Momentum (BE-M) models for the design and analysis of vertical-axis wind turbines has aroused a large credit both in research and academic communities as well as in industry, thanks to general acceptable accuracy of the results, widely available literature and code simplicity.

As focused by Burton et al. [1], the basic assumption of the BE-M theory is that the forces acting on a blade element, calculated by means of two-dimensional airfoil characteristics on the basis of a local angle of attack determined from the incident resultant velocity in the cross sectional plane of the rotor, are responsible for the change in momentum of the air which flows through the streamtube containing the blade element itself. It is therefore to be assumed that there is no radial interaction between the flows through contiguous streamtubes.

The BE-M theory was first introduced by Glauert [2] for predicting the structural dynamics and performance of airplane propellers.

Marco Raciti Castelli is a Research Associate at the Department of Mechanical Engineering of the University of Padua, Via Venezia 1, 35131 Padova, Italy (e-mail: marco.raciticastelli@unipd.it).

Andrea Fedrigo has completed his M.Sc. in Mechanical Engineering at the University of Padua, Via Venezia 1, 35131 Padova, Italy.

Ernesto Benini is an Associate Professor at the Department of Mechanical Engineering of the University of Padua, Via Venezia 1, 35131 Padova, Italy (e-mail: ernesto.benini@unipd.it).

Templin [3] adjusted the momentum based model for vertical-axis wind turbine aerodynamics, obtaining the most elementary approach based on momentum theory, named Single-Streamtube model. As reported by Klimas [4], this approach established a streamtube bounded by the rotor and equated the loss of air windwise momentum to the circumferentially averaged windwise gain in momentum of the blades. Calculations were performed for a single blade whose chord equaled the sum of the chords of the actual rotor's blade, while upwind and downwind passages of the blade through the streamtube were considered in an averaged sense as well, therefore only an average torque per revolution was predictable.

As focused by Claessens [5], Single-Streamtube model was developed in two directions: the first one was splitting the single streamtube in a number of parallel streamtubes, resulting in the Multiple-Streamtube model, the other direction was the double actuator disk analysis, which places two actuator disks in tandem formation, resulting in two different interference factors for the upwind part of blade revolution and for the downwind one. These models were eventually combined in the Double Multiple-Streamtube (DMS) model.

Strickland [6] extended Templin's approach by considering the single streamtube to be composed of a number of adjacent and aerodynamically independent smaller streamtubes, thus allowing element airfoil characteristics based on local (rather than on average) Reynolds number to be used and also the effects of wind shear to be considered. This approach, named Multiple-Streamtube model, proved to be able to predict the performance of small scale rotors much more accurately than the Single-Streamtube model and was able to simulate also the distribution of aerodynamic forces along rotor blades as a function of azimuthal position, thus proposing itself as a powerful engineering design tool for studying the effects of rotor geometry variations, such as blade solidity, blade taper and variations in rotor aspect ratio.

The main disadvantage of Multiple-Streamtube model is its inherent inability to distinguish between upwind and downwind period of blade revolution, thus forcing an unrealistic symmetry of aerodynamic loads between the two passages of the blade element into the same streamtube. As previously discussed, further improvements in the Multiple-Streamtube model have been performed by several authors [7], [8], [9], [10], [11] by placing two actuator disks behind each other, thus allowing to model also velocity variations in the direction perpendicular to the freestream flow between the upwind part of the turbine and the downwind one. The resulting approach, named Double Multiple-Streamtube

model, obtained by combining the multiple streamtube model with the double actuator disk theory, is the most advanced performance prediction tool based on momentum theory.

The present work adopts a multiple-option Single/Double disk Multiple-Streamtube model linked to a numerical algorithm, capable of generating the desired rotor conformation depending on the design geometric parameters. Element airfoil characteristics, based on local Reynolds number, are obtained through interpolation of literature low-Reynolds airfoil databases from Sheldal and Klimas [12], who performed low turbulence wind tunnel measurements at moderate Reynolds values, in order to obtain extended (up to 180° angles of attack) databases of some classical NACA airfoils for vertical-axis wind turbine applications.

Some corrections are introduced inside the model, with the aim of improving the original code prediction capabilities by simulating also the effects of blade dynamic stall, rotor streamtube expansion and blade finite aspect ratio, for which a new empirical relationship to better fit the experimental data is proposed. After describing and validating the model against experimental data, a computational campaign is carried out for a troposkien rotor architecture for which experimental data are available in literature [13], [14], allowing a comparison between the code prediction capabilities as a function of the above described corrections. Referring experimental data to open field rotor operation, a freestream wind shear profile is implemented in the model, thus reproducing the effect of atmospheric boundary layer.

II. MODEL DESCRIPTION

Fig. 1 shows a schema of the adopted survey methodology, consisting in the coupling of an analytical code for rotor geometry definition to a mesh generator, which is linked to a Single/Double-Disk Multiple-Streamtube BE-M code for the calculation of rotor performance.

The numerical code is based upon an adaptation of Glauert [2] blade element theory, adopting the streamwise momentum equation for a series of streamtubes passing through the rotor cross-sectional area, giving rise to a non-uniform distribution of flow velocities.

A numerical algorithm has been developed, capable of generating the desired rotor conformation depending on design geometric parameters: four options have been implemented for rotor geometry, in order to be able to process all of the most used turbine architectures:
1. straight blades;
2. single curvature blades;
3. SCS blades (i.e. Straight-Circular-Straight blades, being an approximation of the Troposkien geometry);
4. general geometry blades, implementable into the code through a User-Defined-Function.

Also spokes have been considered and four options have been implemented:
1. no spokes;
2. a single spoke placed at rotor midsection;

3. two spokes placed symmetrically with respect to rotor midsection;
4. three spokes, one of which placed at rotor midsection and the other two placed symmetrically with respect to rotor midsection.
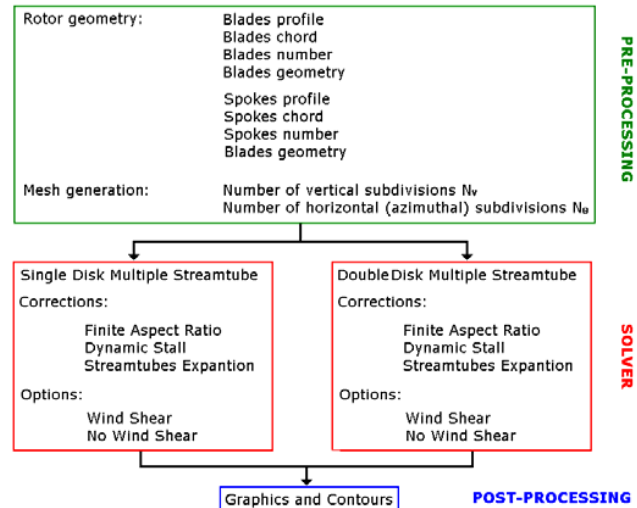

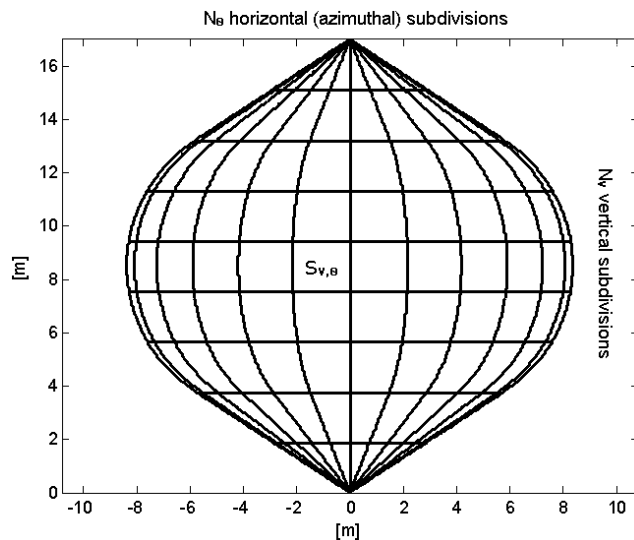Fig. 1 Schema of the adopted survey methodology

Fig. 2 Schematic view of the mesh generation for a SCS rotor

Through the pre-processing mesh algorithm it is possible to control both the number of vertical subdivisions N_v and the number of horizontal (azimuthal) subdivisions N_θ. A schematic view of the mesh generation process for a SCS rotor architecture is shown in Fig. 2.

Fig. 3 presents a drawing of the induced velocities through the rotor for Single-Disk Multiple-Streamtube code configuration. Referring to every single streamtube, whose cross-sectional area is assumed to be constant as it passes through the rotor, three characteristic flow velocities can be considered: the freestream unperturbed wind speed $V_{\infty,wind}$, the

freestream wake velocity $V_{\infty,wake}$ and the actual velocity at blade section V_{blade}. Since energy is extracted by the blade elements as they pass through the streamtube, the following relation can be written between the three characteristic flow velocities:

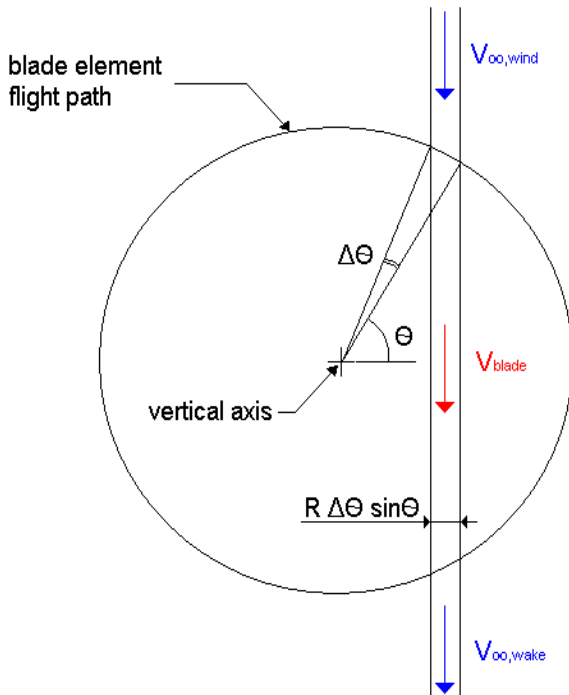$$V_{\infty,wind} > V_{blade} > V_{\infty,wake} \qquad (1)$$

Fig. 3 Plan view of rotor cross-section and visualization of the three streamtube characteristic flow velocities for Single-Disk Multiple-Streamtube configuration

As can be seen from Figs. 2 and 3, the total span of the single streamtube bounded by the rotor is subdivided into several streamtubes using a fixed angle $\Delta\theta$ in order to cluster the streamtube density distribution close to rotor cross-section borders, in formulas:

$$\Delta\theta = 2\pi/N_\theta \qquad (2)$$

$$L_s = R\,\Delta\theta\,\sin\theta \qquad (3)$$

From Strickland's model [6], for each single streamtube, the time averaged streamwise momentum equation can be used in conjunction with Bernoulli's equation to relate the three streamtube characteristic flow velocities and the averaged streamwise force exerted by the blade elements as they pass through the streamtube, in formulas:

$$F_{x,ave} = 2\,m'\,(V_{\infty,wind} - V_{\infty,out}) = 2\,\rho\,A_s\,V_{blade}\,(V_{\infty,wind} - V_{blade}) \qquad (4)$$

being the velocity in the rotor plane the mean of the freestream

unperturbed wind speed and the freestream wake velocity [15]:

$$V_{blade} = (V_{\infty,wind} + V_{\infty,wake})/2 \qquad (5)$$

Still according to Strickland [6], being $\Delta\theta/2\pi$ the probability for the blade element to be inside each streamtube, the relationship between the average streamwise force inside the streamtube and the streamwise force exerted by an individual blade element is:

$$F_{x,ave} = N\,F_x\,\Delta\theta/2\pi \qquad (6)$$

and, eliminating $F_{x,ave}$ from eq. (4) and (6), the following relation can be determined:

$$\frac{NF_x}{2\pi\rho r\Delta h \sin\theta V_{\infty,wind}^2} = \frac{V_{blade}}{V_{\infty,wind}}\left(1 - \frac{V_{blade}}{V_{\infty,wind}}\right) \qquad (7)$$
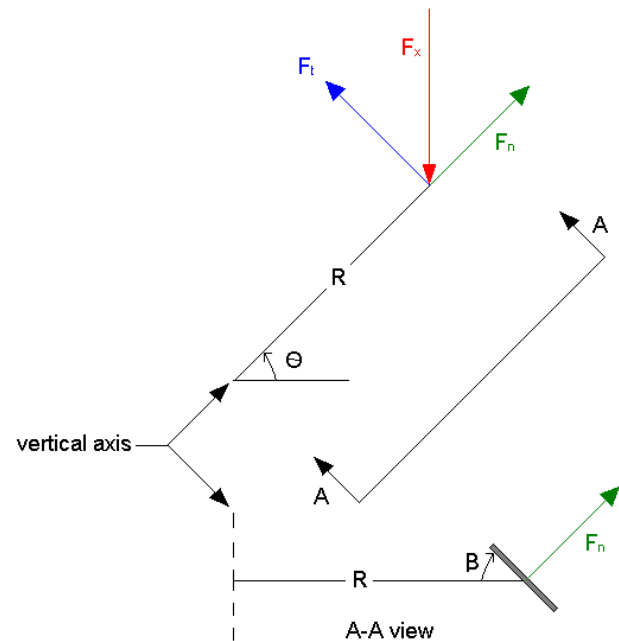

Fig. 4 Plan view of rotor cross-section and vertical section for visualization of blade element tangential and normal forces, along with their resultant in streamwise direction

Blade element tangential and normal forces, along with their resultant in streamwise direction, are shown in Figure 4, in formulas:

$$F_t = \tfrac{1}{2}\,Ct\,\rho\,\Delta h\,c/\sin\beta\,W^2 \qquad (8)$$

$$F_n = -\tfrac{1}{2}\,Ct\,\rho\,\Delta h\,c/\sin\beta\,W^2 \qquad (9)$$

$$F_x = -(F_n \sin\beta \sin\theta + F_t \cos\theta) \qquad (10)$$

being c the blade element chord length, W the relative velocity in blade element cross-sectional plane, C_t and C_n the tangential and normal force coefficients, which are related to blade lift

and drag coefficients by the following relations:

$$C_t = C_L \sin\alpha - C_D \cos\alpha \tag{11}$$

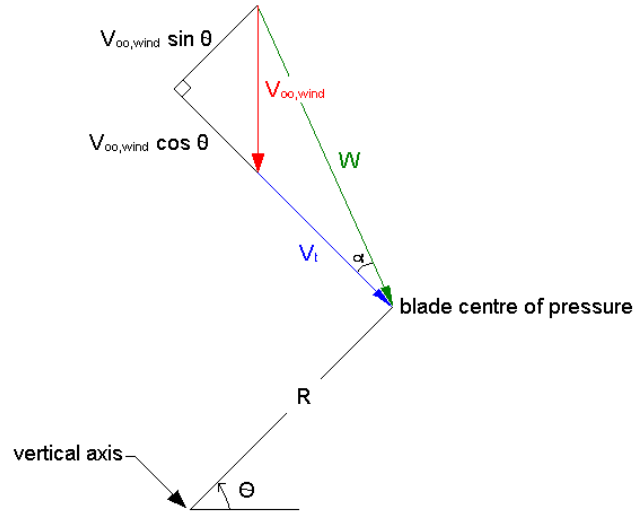$$C_n = C_L \cos\alpha + C_D \sin\alpha \tag{12}$$

Fig. 5 Blade element characteristic velocities and angles on plan view of rotor cross-section

Defining the non-dimensional streamwise force as:

$$F_x^* = \frac{NF_x}{2\pi\rho r\Delta h \sin\theta V_{\infty,wind}^2} \tag{13}$$

and combining eqs. (7), (8), (9) and (10), the following relation can be written:

$$F_x^* = \frac{Nc}{4\pi r}\left(\frac{W}{V_{\infty,wind}}\right)^2\left(C_n - C_t\frac{\cos\theta}{\sin\theta\sin\beta}\right) \tag{14}$$

Fig. 5 shows blade element characteristic velocities and angles. Being V_t blade element tangential speed, blade element local angle of attack can be written as:

$$\alpha = \operatorname{arctg}\frac{V_{blade}\sin\theta\sin\beta}{V_{blade}\cos\theta + V_t} \tag{15}$$

being

$$V_t = \omega r \tag{16}$$

and the relative velocity in blade element cross-sectional plane can consequently be written as:

$$W = \frac{V_{blade}\sin\theta\sin\beta}{\sin\alpha} \tag{17}$$

Defining the axial induction factor as:

$$a = 1 - \frac{V_{blade}}{V_{\infty,wind}} \tag{18}$$

and considering eqs. (7), (13), the streamwise momentum

equation can be written as:

$$a = F_x^* + a^2 \tag{19}$$

forming the basis for an iterative solution. For values of axial induction factor higher than 0.5, Glauert's correction [16] has been implemented in the code.

Once the streamtube momentum equation has been solved, blade element torque for each streamtube can be determined by:

$$T_s = \frac{1}{2}\rho r C_t \frac{c\Delta h}{\sin\beta}W^2 \tag{20}$$

and the average torque produced by a complete blade during a full revolution is obtained by the sum of the contributions given by all blade elements, averaging the resulting values of all angular positions:

$$T_{ave,single\,bl} = \frac{1}{N_\theta}\sum_1^{N_a}\sum_1^{N_v}T_s \tag{21}$$

Average rotor torque is consequently given by:

$$T_{ave} = N\,T_{ave,single\,bl} \tag{22}$$

average rotor power by:

$$P_{ave} = T_{ave}\,\omega \tag{23}$$

and average rotor power coefficient by:

$$C_{P,ave} = \frac{P_{ave}}{1/2\rho A V_{\infty,wind}^2} \tag{24}$$

being A the rotor swept area.

Fig. 6 presents a drawing of the induced velocities through the rotor for Double-Disk Multiple-Streamtube configuration. As focused by Masson et al. [17], the flow in each streamtube is considered to be acted upon by two actuator disks: the first one representing the upwind half of the surface swept by the rotor blades ($0 \le \theta \le \pi$) and the second one representing the downwind half of the rotor ($\pi \le \theta \le 2\pi$). The upwind component and the downwind one, which travel across each streamtube, are considered separately and in the middle plane between upstream rotor zone and the downstream one an equilibrium-induced velocity is considered. Referring to every single streamtube, whose cross-sectional area is assumed to be constant as it passes through the rotor, five characteristic flow velocities can be considered: the freestream unperturbed wind speed $V_{\infty,wind}$, the actual velocity at blade section $V_{blade,up}$ during upwind passage, the equilibrium-induced velocity in the middle plane between upstream and downstream rotor zones V_{eq}, the actual velocity at blade section $V_{blade,down}$ during downwind passage and the freestream wake velocity $V_{\infty,wake}$. Since energy is extracted by the blade elements as they pass through the streamtube, the following relation can be written between the five characteristic flow velocities:

$$V_{\infty,wind} > V_{blade,up} > V_{eq} > V_{blade,down} > V_{\infty,wake} \qquad (25)$$
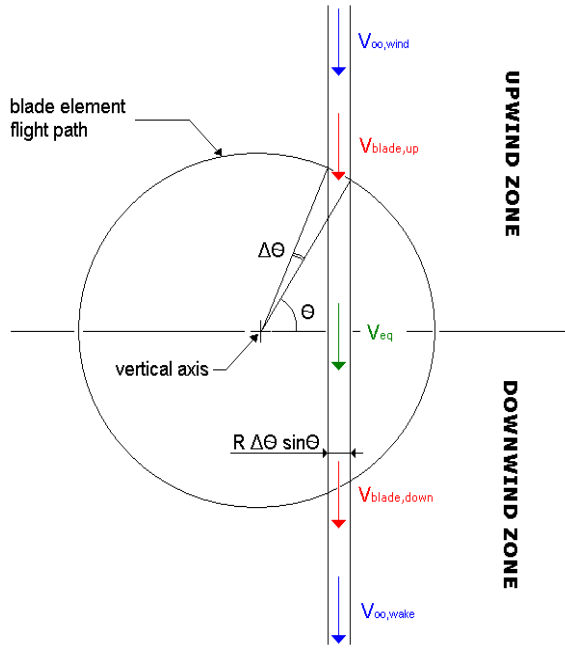

Fig. 6 Plan view of rotor cross-section and vizualization of the five streamtube characteristic flow velocities for Double Disk Multiple Streamtube configuration

The same mathematical formulation adopted for the Single-Disk architecture is repeated for the Double-Disk one, with the only variation of eq. (14), which, due to the fact that each actuator disk is seeing just one flow crossing, is equal to:

$$F_x^* = \frac{Nc}{8\pi r}\left(\frac{W}{V_{\infty,wind}}\right)^2 \left(C_n - C_t \frac{\cos\theta}{\sin\theta\sin\beta}\right) \qquad (26)$$

III. DYNAMIC STALL CORRECTION

Dynamic stall is a non-linear unsteady aerodynamic effect that occurs when blade profiles rapidly change their angle of attack. This sudden change can cause a strong vortex to be shed from the leading edge of the airfoil, and travel backwards above the blade [17]. The vortex, containing high velocity airflows, briefly increases the lift produced by rotor blades. In such conditions, the dynamic lift and drag characteristics present a hysteresis response which is completely different from the static coefficients.

As focused by Masson et al. [18], the aim of a dynamic stall model is to propose a methodology to compute the dynamic characteristics from the available experimental static coefficients.

Gormont [19] first developed a dynamic stall model for helicopter blades, by empirically reproducing the hysteresis response of an airfoil through the definition of a reference angle of attack, different from the geometric one, at which the static two-dimensional data are considered.
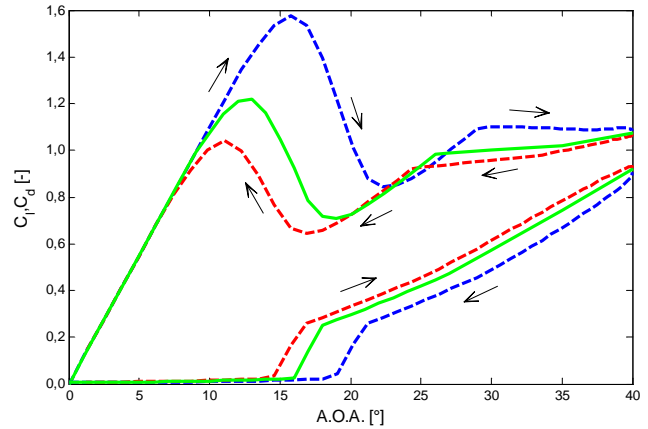

Fig. 7 NACA 0012 lift and drag static (green) and dynamic (blue and red) coefficients as a function of the angle of attack – Strickland dynamic stall model, Re = 2.000.000
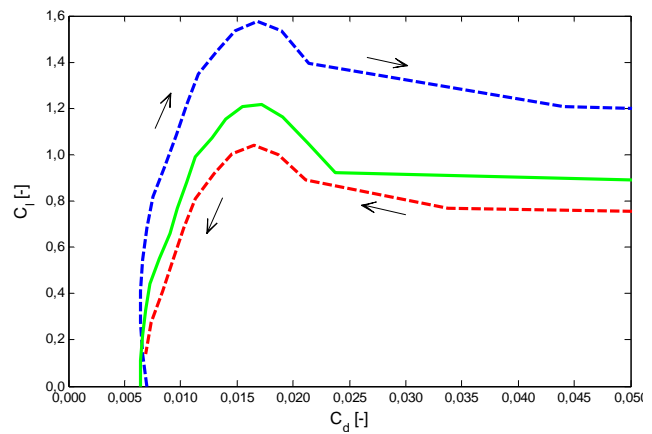

Fig. 8 NACA 0012 static (green) and dynamic (blue and red) polars – Strickland dynamic stall model, Re = 2.000.000

Strickland et al. [20] proposed an adaption of the Gormont model for vertical-axis wind turbine applications, considering also the flow to be incompressible.

In order to avoid some overprediction of dynamic stall effects close to very high blade angles of attack, Massé [21] proposed a modification of the original Gormont model, based on a linear interpolation between the dynamic coefficients predicted by Gormont model and the static coefficients. Starting from Massé's modification, Berg [22] proposed a new coefficient in order to take dynamic effects into account. For a detailed description of the evolution of dynamic stall models, see [18].

In the present work, both Strickland and Berg corrections have been implemented in the model. Figs. from 7 to 10 show the effects of dynamic stall on a NACA 0012 lift and drag coefficients for a constant speed of angle of attack variation (both positive and negative). As can be seen, the hysteresis cycle computed using Berg dynamic stall model is narrower with respect to Strickland model.
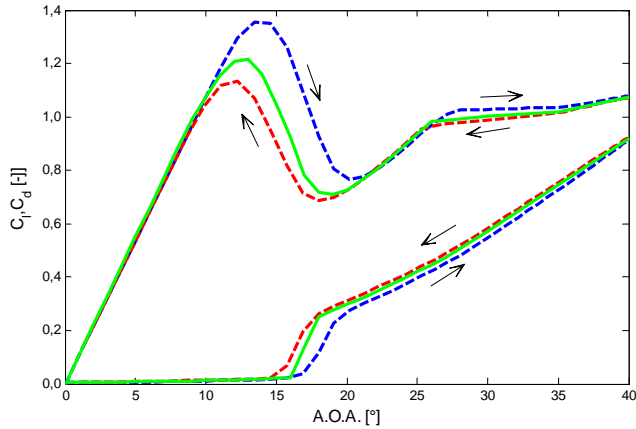
Fig. 9 NACA 0012 lift and drag static (green) and dynamic (blue and red) coefficients as a function of the angle of attack – Berg dynamic stall model, Re = 2.000.000
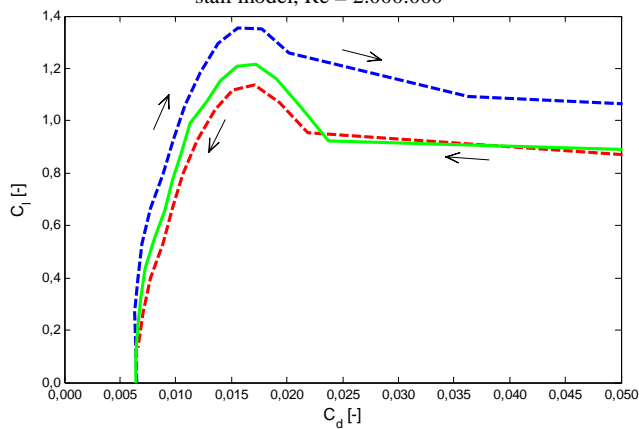

Fig. 10 NACA 0012 static (green) and dynamic (blue and red) polars – Berg dynamic stall model, Re = 2.000.000

IV. STREAMTUBE EXPANSION CORRECTION

Because of work exchange between fluid and blade element in the upwind part of blade revolution, the flux of kinetic energy flowing into each streamtube is reduced and the downwind part of the rotor experiences lower flow velocities [23]. Being the flow considered incompressible, the continuity equation compels the streamtube to expand, as is shown in Fig. 11. In order to consider streamtube expansion, which was first applied to vertical-axis wind turbines by Read and Sharpe [24], two equilibrium-induced velocities in the middle plane between upstream and downstream rotor zones must be considered, both for upwind and downwind.
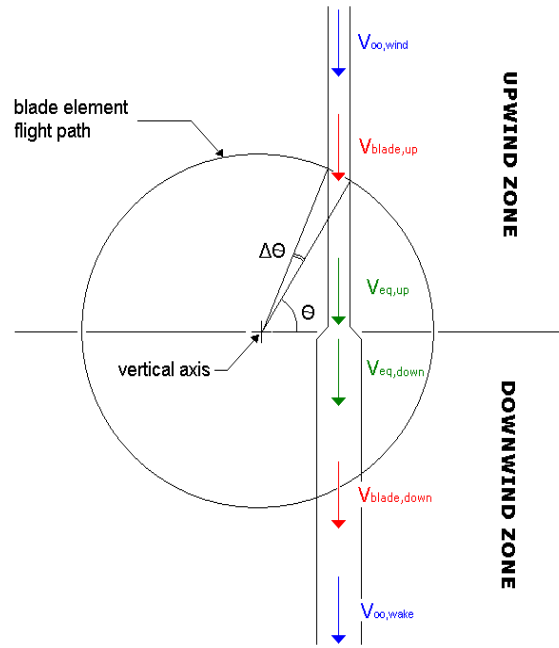

Fig. 11 Plan view of rotor cross-section and vizualization of the six streamtube characteristic flow velocities for Double-Disk Multiple-Streamtube configuration with streamtube expansion correction
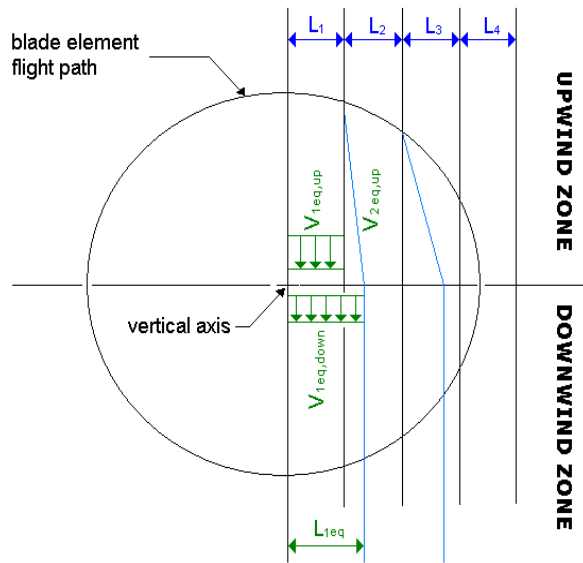

Fig. 12 Determination of the downwind equilibrium-induced velocity

Fig. 12 presents the procedure for the calculation of the downwind equilibrium-induced velocity, which is the result of a weighted averaging of all the upwind equilibrium-induced velocities which insist on the downwind part of the streamtube.

With reference to Fig. 12, the downwind equilibrium-induced velocity for streamtubes No. 1 and No. 2 can be obtained by the following relations:

$$V_{1eq,down} = V_{1eq,up} \tag{27}$$

$$V_{2eq,down} = \frac{V_{1eq,up}(L_{1eq} - L_1) + V_{2eq,up}(L_1 + L_2 - L_{1eq})}{L_2} \quad (28)$$

if $\qquad L_1 + L_2 - L_{1eq} > 0$

and:

$$V_{2eq,down} = V_{1eq,up} \quad (29)$$

if $\qquad L_1 + L_2 - L_{1eq} < 0$

These velocities are used as an input for the resolution of the downwind part of the streamtubes.

V. FINITE ASPECT RATIO CORRECTION

Airfoil databases, such as those from Sheldal and Klimas [12], are only available for infinite aspect ratios. For finite rotor blade aspect ratio conditions, defined as:

$$A.R. = L_b/c \quad (30)$$

the lift coefficient results always lower than the corresponding infinite airfoil coefficient while the drag coefficient results higher for small angles of attack and lower when angles of attack exceed the stall.
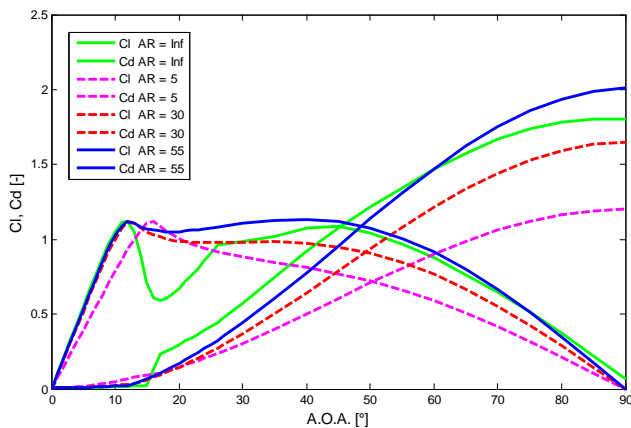

Fig. 13 NACA 0012 lift and drag coefficients as a function of the angle of attack for different values of blade aspect ratio - Viterna and Corrigan model, Re = 1.000.000

Lift and drag coefficients for finite aspect ratio airfoils at small angles of attack before stall can be estimated quite accurately from infinite aspect ratio airfoil data by using the Lanchester Prandtl theory [25].

Viterna and Corrigan model [26] provides a mean to modify the airfoil data after the stalling angle of attack and up to 90°. After the infinite airfoil characteristics data has been modified by Lanchester Prandtl theory, this model is able to estimate the lift and drag coefficients after stall. However, while model predictions result quite good for stalled condition, as the

maximum lift coefficient (at stall) remains the same (only angle of attack increases) from the previous Prandtl modification, the correction results in a higher lift coefficient after the stall point (around the lift dip) with respect to the infinite span airfoil, as can be seen from Fig. 13.
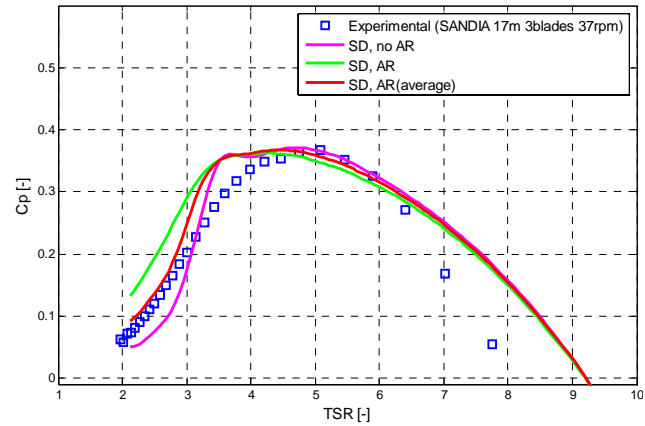

Fig. 14 Comparison between experimental data from [14] and Single-Disk Multible-Streamtube model prediction. The averaging between Viterna/Corrigan correction and infinite aspect ratio airfoil database proves to fit experimental data best

The overestimation of the lift coefficient after the stall angle, together with the decrease of the drag coefficient can determine a fictitious overestimation of rotor performance, as can be seen in Fig. 14 for a Single-Disk Multiple-Streamtube model. In order to avoid this overprediction, the present work proposes to compute modified finite aspect ratio airfoil characteristics based on a linear interpolation between the 2D values of airfoil lift and drag coefficients and the finite aspect ratio coefficients predicted by the Viterna and Corrigan model, in formulas:

$$C_L = \frac{C_{L,A.R.=\infty} + C_{L,Viterna/Corrigan}}{2} \quad (31)$$

$$C_D = \frac{C_{D,A.R.=\infty} + C_{D,Viterna/Corrigan}}{2} \quad (32)$$

Fig. 14 displays the evolution of the power coefficient, defined as:

$$C_p = \frac{P}{1/2\rho A V_{\infty,wind}^2} \quad (33)$$

as a function of the tip speed ratio, defined as:

$$TSR = \omega R/V_{\infty,wind} \quad (34)$$

for Sandia 17 m diameter SCS rotor [14]. As can be clearly seen, this new empirical adaptation of the Viterna and Corrigan model proves to fit the experimental measurements better, especially for lower values of tip speed ratios, where rotor blades experience higher angles of attack.
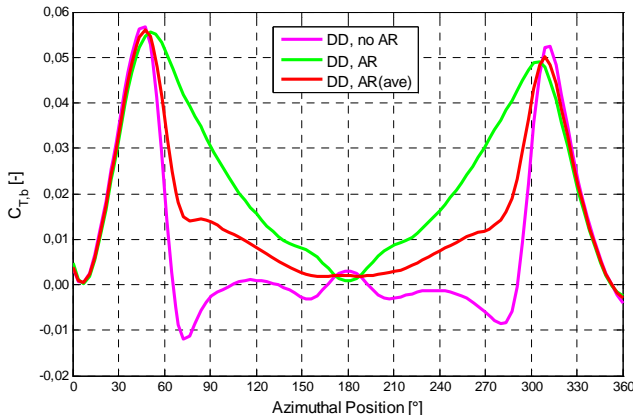
Fig. 15 Distribution of the istantaneous blade torque coefficient as a function of azimuthal position for Sandia three-bladed 17 m diameter SCS rotor [14]; TSR = 2
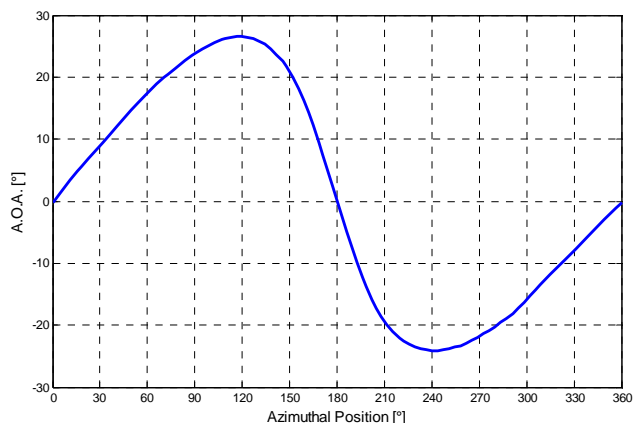

Fig. 16 Distribution of the local blade angle of attack as a function of azimuthal position for Sandia three-bladed 17 m diameter SCS rotor [14]; TSR = 2

Figs. 15 and 16 show the distribution of the instantaneous blade torque coefficient, defined as:

$$C_{T,b}(\theta) = \frac{M_b(\theta)}{1/2\rho A V_{\infty,wind}^2 R} \qquad (35)$$

and of local blade angle of attack as a function of azimuthal position for a TSR of 2, that is where greater differences between the dynamic stall models are registered. As can be clearly seen, for azimuthal position where the blades experience higher angles of attack (between 60° and 160° for upwind angular position and between 200° and 300° for downwind angular position), the three model predictions are completely different, resulting the proposed averaging between Viterna and Corrigan correction half-way between the other two models.

Further research is to be performed in order to validate the proposed empirical correction by comparison between experimental instantaneous blade torque coefficient distribution and BE-M predictions.

VI. FREESTREAM WIND PROFILE IMPLEMENTATION

Referring most of literature about vertical-axis wind turbine experimental data to open field rotor operation, a freestream wind shear profile has been implemented in the model, thus reproducing the effect of atmospheric boundary layer.

As shown in Fig. 17, the velocity profile is computed using the following relation, determining the freestream unperturbed wind velocity for each streamtube as a function of the height with respect to ground level:

$$V_{\infty,wind} = (y + \frac{H_0}{H/2} + H_0)V_{ref} \qquad (36)$$

being y the vertical distance between the streamtube section midpoint and the base of the rotor, H rotor height, H_0 the height of the turbine mast (considering the mast to extend just up to lower rotor section) and V_{ref} the reference velocity for the examined operating conditions. Eq. (36) is calibrated so as to have $V_{\infty,wind} = V_{ref}$ at rotor midsection as well as $V_{\infty,wind} = 0$ at ground level.
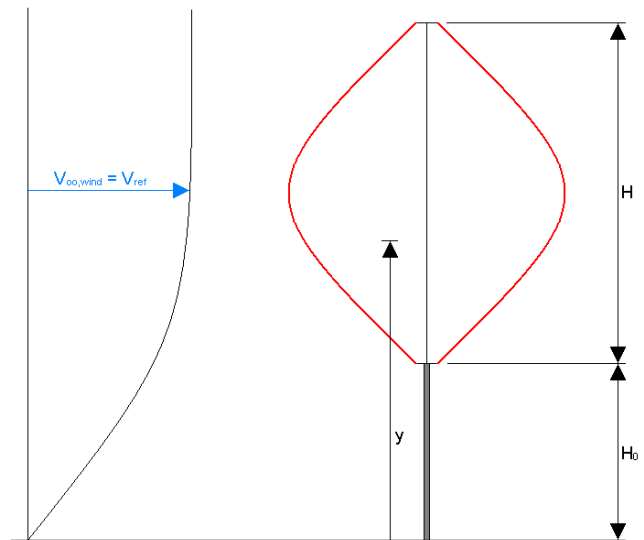

Fig. 17 Main parameters for calculation of wind shear

VII. RESULTS AND DISCUSSION

Fig. 18 displays the power coefficient as a function of the tip speed ratio for Sandia 17 m diameter SCS rotor [14]. As can be clearly seen, being no correction implemented in the code, Single-Disk Multiple-Streamtube model is able to capture the experimental data better with respect to the corresponding Double-Disk model, whose prediction capabilities result quite poor.
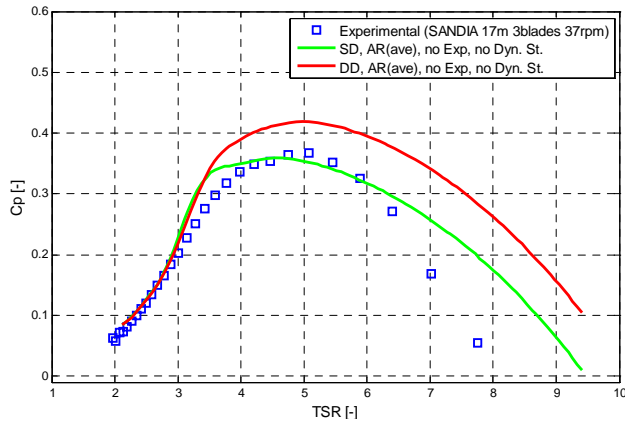
Fig. 18 Comparison between experimental data from [14], Single-Disk and Double-Disk Multible-Streamtube model prediction
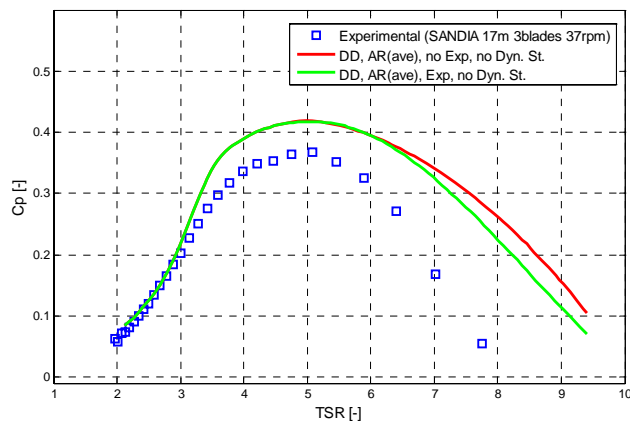

Fig. 19 Effect of streamtube expansion correction on Double-Disk Multible-Streamtube model prediction capabilities for Sandia three-bladed 17 m diameter SCS rotor [14]
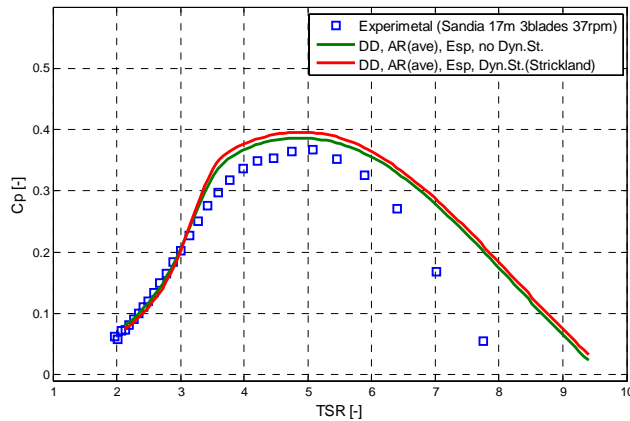

Fig. 20 Effect of Strickland dynamic stall correction on Double-Disk Multible-Streamtube model prediction capabilities for Sandia three-bladed 17 m diameter SCS rotor [14]

Fig. 19 displays the power coefficient as a function of the tip speed ratio for the Double-Disk model, where streamtube expansion correction has been implemented. As can be seen, the code prediction capability is enhanced for the region of high values of TSR, where the streamtubes expansion phenomenon is prevailing. No difference can be registered for low values of TSR.
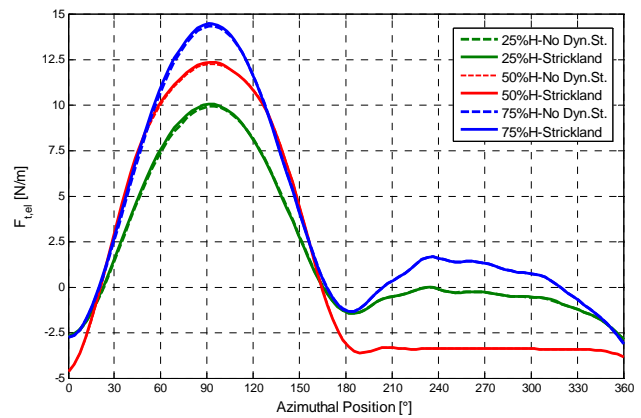

Fig. 21 Effect of Strickland dynamic stall correction on blade element tangential forces per unit length for Sandia three-bladed 17 m diameter SCS rotor [14] at different values of rotor circumferential sections; TSR = 8.23
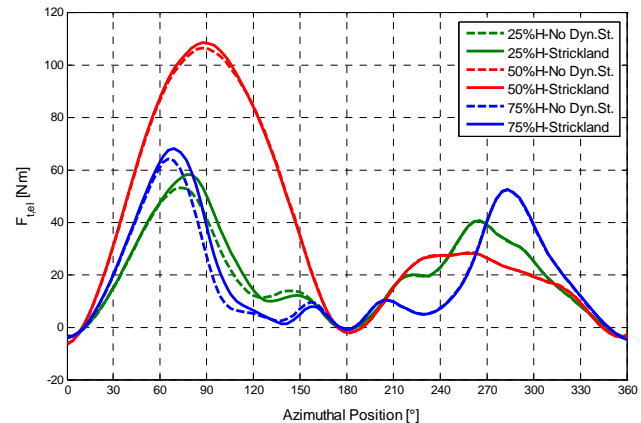

Fig. 22 Effect of Strickland dynamic stall correction on blade element tangential forces per unit length for Sandia three-bladed 17 m diameter SCS rotor [14] at different values of rotor circumferential sections; TSR = 4.12

Fig. 20 displays the power coefficient as a function of the tip speed ratio for the Double-Disk model where Strickland dynamic stall correction has been implemented. As can be seen, Strickland's model fails in reproducing experimental data (Strickland's model corrected predictions are worse than the original model without any correction) because of overestimation of rotor performance.

Figs. 21 to 23 reproduce blade element tangential forces per unit length as a function of blade azimuthal position, for different values of rotor circumferential sections and for several rotor tip speed ratios. The effect of atmospheric wind shear is also considered. It can be clearly seen that Strickland dynamic stall model influences the upwind sector of blade revolution, being almost ininfluential for the downwind sector. It is also clear that the effect of dynamic stall is predominant at

low values of TSR, where rotor blades experience higher angles of attack. Because of the combined effects of atmospheric wind shear, local radius and local values of TSR, rotor sections at 25%, 50% and 75% rotor height can perform quite differently.
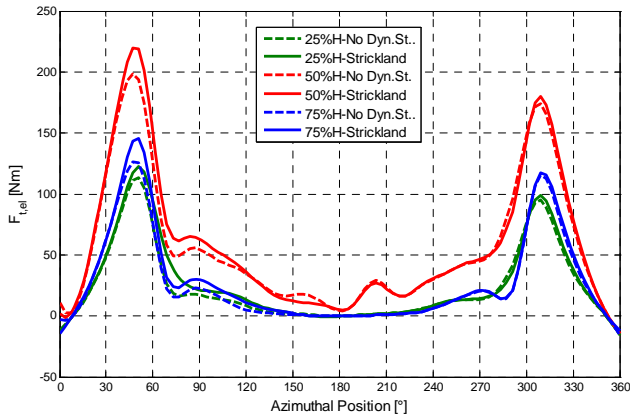

Fig. 23 Effect of Strickland dynamic stall correction on blade element tangential forces per unit length for Sandia three-bladed 17 m diameter SCS rotor [14] at different values of rotor circumferential sections; TSR = 2.35

Fig. 24 displays the power coefficient as a function of the tip speed ratio for the Double-Disk model and Berg dynamic stall correction. It can be seen that Berg dynamic stall model prediction capabilities are quite good.
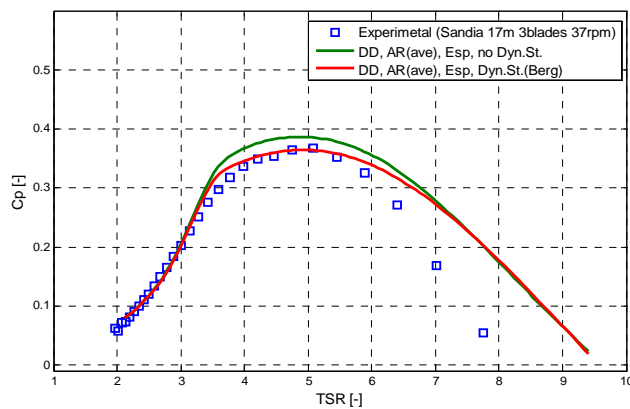

Fig. 24 Effect of Berg dynamic stall correction on Double-Disk Multible-Streamtube model prediction capabilities for Sandia three-bladed 17 m diameter SCS rotor [14]

Figs. 25 to 27 reproduce blade element tangential forces per unit length as a function of blade azimuthal position, for different values of rotor circumferential sections and for several rotor tip speed ratios. The effect of atmospheric wind shear was also considered. It can be clearly seen that Berg dynamic stall model influence both the upwind sector of blade revolution and the downwind one. Also for this case, because of the combined effects of atmospheric wind shear, local radius and local values of TSR, rotor sections at 25%, 50% and 75% rotor height can perform quite differently.
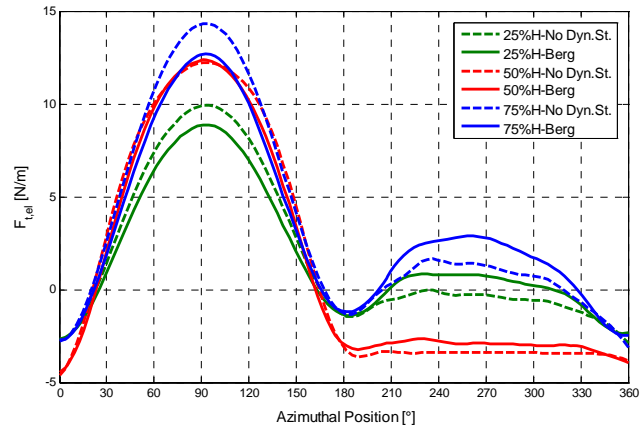

Fig. 25 Effect of Berg dynamic stall correction on blade element tangential forces per unit length for Sandia three-bladed 17 m diameter SCS rotor [14] at different values of rotor circumferential sections; TSR = 8.23

Fig. 26 Effect of Berg dynamic stall correction on blade element tangential forces per unit length for Sandia three-bladed 17 m diameter SCS rotor [14] at different values of rotor circumferential sections; TSR = 4.12

By comparing Figs. from 21 to 23 with Figs. from 25 to 27 it can be clearly seen that, while Strickland's model tends to enhance blade performance with respect to the original uncorrected code, Berg's model determines a reduction of blade performance for the upwind angular period of revolution, causing a consequent increase of overall blade performance for the downwind period.

Fig. 28 compares Strickland and Berg dynamic stall models prediction capabilities: Berg's model higher performances are quite evident.
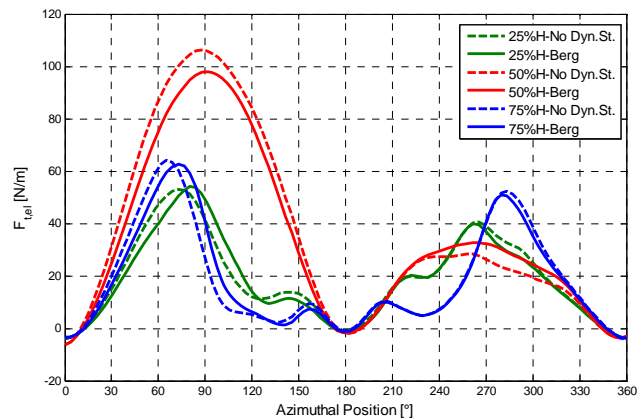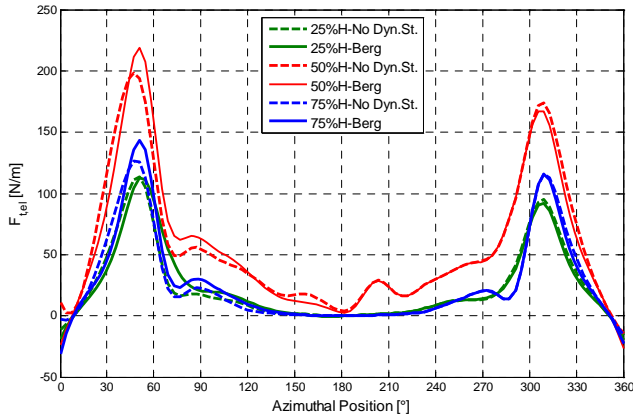
Fig. 27 Effect of Berg dynamic stall correction on blade element tangential forces per unit length for Sandia three-bladed 17 m diameter SCS rotor [14] at different values of rotor circumferential sections; TSR = 2.35
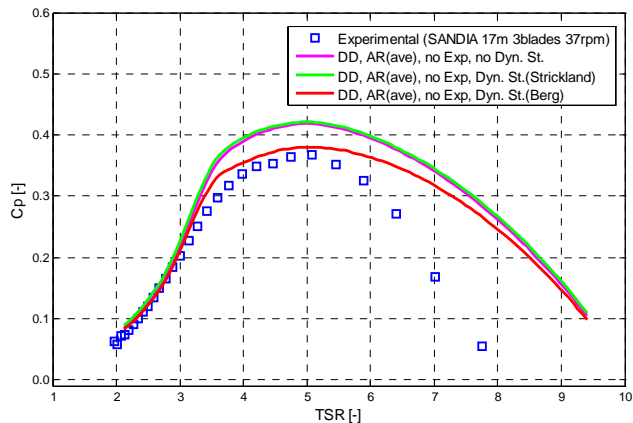

Fig. 28 Comparison between Strickland and Berg dynamic stall model prediction capabilities for Sandia three-bladed 17 m diameter SCS rotor [14]
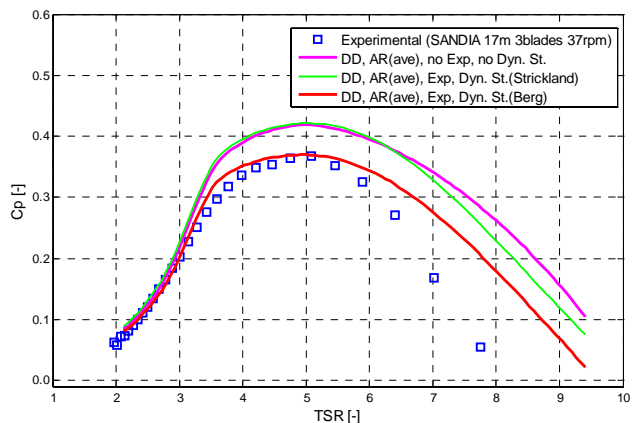

Fig. 29 Evolution of BE-M prediction capabilities with the implementation of code corrections for Sandia three-bladed 17 m diameter SCS rotor [14]

Fig. 29 shows the evolution of the Double-Disk BE-M prediction capabilities with the implementation of highly-refined correction models. As it can be clearly seen, the potentials of Double-Disk Multiple-Streamtube model with the average aspect ratio correction, streamtubes expansion correction and Berg dynamic stall model result quite high.

VIII. CONCLUSIONS AND FUTURE WORK

A multiple-option Single/Double-Disk Multiple-Streamtube BE-M model for the evaluation of energy performance and the distribution of aerodynamic loads acting on a vertical-axis Darrieus wind turbine depending on rotor architecture and operating conditions was presented. In order to predict also open field rotor operation, a freestream wind shear profile was implemented, reproducing the effect of atmospheric boundary layer.

Being no correction implemented in the code, Single-Disk Multiple-Streamtube model was able to better capturing the experimental data with respect to the corresponding Double-Disk configuration, whose prediction capabilities resulted quite poor.

By introducing some corrections inside the original code, with the aim of simulating also the effects of blade dynamic stall, rotor streamtube expansion and blade finite aspect ratio, a strong improvement was noticed in Double-Disk Multiple-Streamtube model capability of reproducing experimental data.

Strickland dynamic stall model resulted inappropriate in simulating the rotor behavior because of an overestimation of overall turbine performance, while Berg model proved able to better predict measured data.

Viterna and Corrigan correction model for finite rotor blade aspect ratio proved to be not satisfactory and a new empirical correlation was proposed, based on the computation of modified finite aspect ratio airfoil characteristics through linear interpolation between the 2D values of airfoil lift and drag coefficients and the finite aspect ratio coefficients predicted by the Viterna and Corrigan model.

Further research is to be performed in order to validate the proposed empirical correction for finite aspect ratio by comparison between experimental instantaneous blade torque coefficient distribution and Double-Disk Multiple-Streamtube BE-M predictions.

NOMENCLATURE

A [m^2]	rotor swept area
A_s [m^2]	streamtube cross-sectional area
A.R. [-]	blade aspect ratio
c [m]	blade element chord length
$C_{T,b}(\theta)$	instantaneous blade torque coefficient
C_D [-]	airfoil drag coefficient
$C_{D,\,A.R.=\infty}$ [-]	airfoil drag coefficient for infinite aspect ratio
$C_{D,\,Viterna/Corrigan}$ [-]	calculation of airfoil drag coefficient using the Viterna and Corrigan model
C_L [-]	airfoil lift coefficient
$C_{L,\,A.R.=\infty}$ [-]	airfoil lift coefficient for infinite aspect

ratio

$C_{L, Viterna/Corrigan}$ [-]   calculation of airfoil lift coefficient using the Viterna and Corrigan model

C_n [-]   blade element normal coefficient

C_p [-]   rotor power coefficient

C_t [-]   blade element tangential coefficient

F_n [N]   blade element normal force

F_t [N]   blade element tangential force

$F_{t,el}$ [N/m]   blade element tangential force per unit length

F_x [N]   streamwise force exerted by the blade element as it pass through the streamtube

$F_{x,ave}$ [N]   averaged streamwise force exerted by the blade element as it pass through the streamtube

H [m]   rotor height

H_0 [m]   mast height

Δh [m]   single streamtube height

L_b [m]   rotor blade length

L_s [m]   single streamtube width

L_{eq} [m]   single streamtube width after expansion (for Double Disk architecture with streamtube expansion correction)

m' [kg/s]   mass flow rate through streamtube

$M_b (\theta)$ istantaneous blade torque

N [-]   number of rotor blades

N_θ [-]   number of horizontal (azimuthal) mesh subdivisions

N_V [-]   number of vertical mesh subdivisions

P_{ave} [W]   average power produced by a complete blade during a full revolution

r [m]   rotor radius relative to blade element

R [m]   rotor radius at equatorial plane

T_{ave} [Nm]   average torque produced by a complete blade during a full revolution

$T_{ave,single\ bl}$ [Nm]   blade element torque for each streamtube

T_s [Nm]   blade element torque for each streamtube

TSR [-]   rotor tip speed ratio

V_{blade} [m/s]   flow velocity at blade section (for Single Disk architecture)

$V_{blade,down}$ [m/s]   flow velocity at blade section during downwind passage (for Double Disk architecture)

$V_{blade,up}$ [m/s]   flow velocity at blade section during upwind passage (for Double Disk architecture)

V_{eq} [m/s]   equilibrium-induced velocity in the middle plane between upstream and downstream rotor zones

$V_{eq,down}$ [m/s]   downstream equilibrium-induced velocity in the middle plane between upstream and downstream rotor zones

(for Double Disk architecture with streamtube expansion correction)

$V_{eq,up}$ [m/s]   upstream equilibrium-induced velocity in the middle plane between upstream and downstream rotor zones (for Double Disk architecture with streamtube expansion correction)

V_{ref} [m/s]   reference velocity for the examined operating conditions

V_t [m/s]   blade element tangential speed

$V_{\infty,wind}$ [m/s]   freestream unperturbed wind speed

$V_{\infty,wake}$ [m/s]   freesetream wake velocity

y [m]   vertical distance between the streamtube section midpoint and the base of the rotor

α [°]   blade angle of attack between chord line and relative velocity

β [°]   blade element inclination with respect to horizontal plane

θ [°]   blade azimuthal coordinate

$\Delta\theta$ [°]   fixed azimuthal angle identifying a single streamtube

ρ [kg/m^3]   air density

ω [rad/s]   rotor angular velocity

REFERENCES

[1] T. Burton and D. Sharpe, N. Jenkins and E. Bossanyi, E., *Wind Energy Handbook*, John Wiley & Sons, Ltd, Baffins Lane, Chichester – West Sussex, PO19 1UD, England, 2001, p. 61.

[2] H. Glauert, *Airplane Propellers, Aerodynamic Theory*, Dover Publication Inc, New York, 1963, Vol. 4, Division L, 169-360.

[3] R. J. Templin, *Aerodynamic Theory for the NRC Vertical-Axis Wind Turbine*, NRC of Canada TR LTR-LA-160, 1974.

[4] P. C. Klimas, "Darrieus Rotor Aerodynamics", *Sandia National Laboratories*, Advanced Energy Projects Division 4715, Albuquerque, NM 87185.

[5] M. C. Claessens, *The Design and Testing of Airfoils for Application in Small Vertical Axis Wind Turbines*, Master of Science Thesis, Faculty of Aerospace Engineering, Delft University of Technology, November 9, 2006.

[6] J. H. Strickland, "The Darrieus Turbine: A Performance Prediction Model Using Multiple Streamtube", Sandia Report, *SAND75-0431*.

[7] S. Read and D. J. Sharpe, "An Extended Multiple Streamtube Theory for Vertical Axis Wind Turbines", *Department of M.A.P. Engineering Report*, Kingston Polytechnic, Kingston upon Times, United Kingdom, 1980.

[8] I. Paraschivoiu, "Double-Multiple Streamtube Model for Darrieus Wind Turbines", *NASA Conference Publication 2185*, May 1981.

[9] I. Paraschivoiu and F. Delclaux, "Double Multiple Streamtube Model with Recent Improvements", *Journal of Energy*, 7(3), 1983, pp. 250-255.

[10] H. Mc Coy and J. L. Loth, "Up- and Downwind Rotor Half Interference Model for VAWT", *AIAA 2nd Terrestrial Energy Systems Conference*, Colorado Springs, CO, December 1-3, 1981.

[11] H. Mc Coy and J. L. Loth, "Optimization of Darrieus Turbines with an Upwind and Downwind Momentum Model", *Journal of Energy*, 7(4), 1983, pp. 313-318.

[12] R. E. Sheldal and C. Klimas, "Aerodynamic Characteristics of Seven Symmetrical Airfoil Sections Through 180-Degree Angle of Attack for Use in Aerodynamic Analysis of Vertical Axis Wind Turbines", *Sandia National Laboratories, Energy Report*, SAND80-2114, March 1981.

[13] M. H. Worstell, "Aerodynamic Performance of the 17 Meter Diameter Darrieus Wind Turbine", Sandia Report, *SAND78-1737*.

[14] M. H. Worstell, "Aerodynamic Performance of the 17-M-Diameter Darrieus Wind Turbine in the Three-Bladed Configuration: An Addendum", Sandia Report, *SAND79-1753*.

[15] M. O. L. Hansen, *Aerodynamics of Wind Turbines*, Earthscan, UK and USA, Second Edition, 2008, p. 30.

[16] H. Glauert, "A General Theory of the Autogyro", *ARCR R&M*, No. 1111, 1926.

[17] K. G. Pierce, *Wind Turbine Load Prediction using the Beddoes-Leishman Model for Unsteady Aerodynamics and Dynamic Stall*, Master of Science Thesis, Department of Mechanical Engineering, The University of Utah, August 1996.

[18] C. Masson, C. Leclerc, and I. Paraschivoiu, "Appropriate Dynamic-Stall Models for Performance Predictions of VAWTs with NLF Blades", *International Journal of Rotating Machinery*, 1998, Vol. 4, No. 2, pp. 129-139.

[19] R. E. Gormont, "An Analytical Model of Unsteady Aerodynamics and Radial Flow for Application to Helicopter Rotors", *U.S. Army Air Mobility Research and Development Laboratory Technical Report*, pp. 72-67, 1973.

[20] J. H. Strickland, B. T. Webster and T. Nguyen, "A Vortex Model of the Darrieus Turbine: an Analytical and Experimental Study", Sandia report, *SAND79-7058*.

[21] B. Massé, "Description de deux programmes d'ordinateur pour le calcul des performance et des charges aérodynamiques pour les éoliennes à axe vertical", *IREQ-2379*, 1981.

[22] D. E. Berg, "An Improved Double-Multiple Streamtube Model for the Darrieus-Type Vertical Axis Wind Turbine", *Sixth Biennal Wind Energy Conference and Workshop*, pp. 231-233.

[23] L. Battisti, A. Brighenti and L. Zanne, "Analisi dell'effetto della scelta dell'architettura palare sulle prestazioni di turbine eoliche ad asse verticale" (in Italian), *64° Convegno ATI*, L'Aquila, Italia, 2009.

[24] S. Read and D. J. Sharpe, "An Extended Multiple Streamtube Theory for Vertical Axis Wind Turbines", *2nd BWEA Workshop*, April 1980.

[25] I. H. Abbot and A. E. Von Doenhoff, *Theory of Wing Sections*, Dover Edition, 1959.

[26] L. A. Viterna and R. D. Corrigan, "Fixed Pitch Rotor Performance of Large Horizontal Axis Wind Turbines", *DOE/NASA Workshop on Large Horizontal Axis Wind Turbines*, 28–30 July 1981, Cleveland, OH.